International Core Journal of Engineering Volume 12 Issue 4, 2026
ISSN: 2414-1895 DOI: 10.6919/ICJE.202604_12(4).0053

Synergistic Mechanisms of Carbonated Bayer Red Mud in Enhancing Chloride Binding Capacity of Cement-Based Materials

Yujie Song, Mifeng Gou*, Yanze Xiong, Jian Lu, Zhen Zhang, Hongxiao Chen, Mingyang Xu

School of Materials Science and Engineering, Henan Polytechnic University, Jiaozuo, 454003, China

*Corresponding Author E-mail: goumifeng@163.com

Abstract

Bayer red mud (BRM), a solid waste, can be effectively treated through carbonation to decrease its alkalinity and improve its reactivity.This study introduces carbonated Bayer red mud (CBRM) as a supplementary cementitious material into the cement system, systematically revealing its influence mechanism on chloride ion (Cl^-) binding behavior and performance optimization pathways in marine environments. The evolution of phase composition and microstructural characteristics during the reaction process of the composite cementitious material system (OPC-CBRM) was analyzed using XRD, TG/DTG, and scanning electron microscopy (SEM).The results showed that compared to ordinary Portland cement paste, the composite cement paste incorporating 30% CBRM exhibited increases of 40% and 68% in total bound chloride and chemically bound chloride contents, respectively, while the physically bound chloride content decreased by 12%.OPC-CBRM generates Friedel's salt (AFm-Cl) efficiently through the release of reactive Al^{3+} (secondary pozzolanic reaction) and the conversion of calcium carbonate to monocarbonate aluminate (AFm-CO_3), followed by Cl^-/CO_3^{2-} ion exchange. The Freundlich model demonstrates a higher goodness-of-fit than the Langmuir model for describing the relationship between free chloride and bound chloride.The presence of Mg^{2+} and Ca^{2+} promotes the decomposition of AFt to form gibbsite. Specifically, Ca^{2+} increases chemically bound chloride content by 24%, while Mg^{2+} increases it by 13%. Sulfate attack reduces chemically bound chloride content: compared with Na_2SO_4 attack, $MgSO_4$ attack results in a 61% reduction, and $CaSO_4$ attack leads to a 60% reduction. It should be noted that CBRM incorporation reduces the compressive strength of cement-based materials, with strength decreasing progressively as CBRM content increases, primarily attributed to reduced C-S-H formation, retarded hydration by Na_2O, and insufficient filler effect of $CaCO_3$. This study provides theoretical foundation for red mud resource utilization and the design of highly durable marine cementitious materials, achieving the dual objectives of "solid waste management for corrosion control" and "carbon sequestration, " which is of significant importance for extending the service life of marine engineering structures.

Keywords

Carbonation; Bayer Red Mud; Chloride Binding; Friedel's Salt; Marine Engineering Materials.

ISSN: 2414-1895 DOI: 10.6919/ICJE.202604_12(4).0053

1. Introduction

Reinforced concrete, as the primary load-bearing structural form, significantly enhances the mechanical properties of concrete. However, chloride-induced corrosion of steel reinforcement in marine environments significantly compromises the durability and service life of reinforced concrete structures[1-5]. According to existing research[6-9], chloride ions in concrete exist in three forms: a. free chloride ions; b. chemically bound chloride ions; c. physically adsorbed chloride ions. The chemical binding of chloride ions primarily occurs through two mechanisms: (i) direct reaction between chloride ions and tricalcium aluminate (C_3A) to form Friedel's salt (FS), or (ii) anion exchange between Cl^- and interlayer anions (SO_4^{2-} or OH^-) in AFm phases ($Ca_4Al_2(SO_4)(OH)_{12}\cdot 6H_2O$) to generate FS ($Ca_4Al_2Cl_2(OH)_{12}\cdot 4H_2O$) or Kuzel's salt (KS) ($Ca_4Al_2(SO_4)_{0.5}Cl(OH)_{12}\cdot 6H_2O$), as illustrated in Equations (1-2)[10, 11].

$$[Ca_2Al(OH)_6]_2(SO_4)(H_2O)_6(AFm) + 2Cl^- \rightarrow [Ca_2Al(OH)_6]_2(Cl)_2(H_2O)_4(FS) + SO_4^{2-} + 2H_2O \quad (1)$$

$$[Ca_2Al(OH)_6]_2(SO_4)(H_2O)_6(AFm) + Cl^- \rightarrow [Ca_2Al(OH)_6]_2(SO_4)_{0.5}(Cl)(H_2O)_6(KS) + 0.5SO_4^{2-} \quad (2)$$

Friedel's salt (FS) and Kuzel's salt (KS) both belong to the layered double hydroxide (LDH) family, with chloride ions intercalated between the layers. Chemical binding does not contribute to chloride-induced corrosion of steel reinforcement[12, 13]. The physical binding of chloride ions mainly involves the adsorption of chloride ions by the electrical double layer structure of C-S-H gel and the adsorption of chloride ions by calcium ions bound to silanol groups. Approximately 20% of chloride ions are physically adsorbed, but this process is reversible[14-16]. In summary, free chloride ions are the key factor in steel reinforcement corrosion[17]. Improving chloride binding capacity can effectively reduce the free chloride content, thereby inhibiting steel corrosion. Therefore, research on enhancing chloride binding capacity is of great significance for extending the service life of reinforced concrete.

In recent years, industrial solid wastes as supplementary cementitious materials (SCMs) have shown significant potential in the field of chloride binding. The incorporation of reactive aluminum-bearing industrial solid wastes, such as slag and fly ash, into cement paste facilitates Friedel's salt formation, thereby enhancing the stability of chemically bound chloride ions[18, 19]. Incorporating 10%–30% barium slag as a SCMs can optimize pore structure, promote Friedel's salt formation, and reduce C-S-H gel generation, thereby enhancing the chloride binding capacity of cement-based materials[20]. Silica fume, as a silicon-rich industrial solid waste with a large specific surface area, can enhance the physical adsorption of chloride ions[21]. However, high-quality fly ash and slag face supply-demand imbalance issues, with price increases exceeding 30%. Some industrial solid wastes require high-temperature activation (such as metakaolin requiring calcination at 800 ℃), which offsets environmental benefits. Furthermore, the chloride binding capacity of conventional industrial solid wastes tends to reach saturation, making it difficult to meet the stringent requirements of harsh marine environments. There is an urgent need to develop new industrial solid waste resources.

Red mud (RM) shows great potential as a supplementary cementitious material. Red mud is an industrial solid waste generated during alumina production, characterized by its distinctive red color[22, 23]. According to production processes, red mud can be classified into three types: Bayer red mud, sintering process red mud, and combined process red mud[24]. Approximately 95% of global alumina enterprises adopt the Bayer process. Currently, the annual discharge of Bayer process red mud is about 180 million tons, with a cumulative total exceeding 4 billion tons[25]. Extensive research has been conducted internationally on the resource utilization of Bayer process red mud, but most remains in the experimental stage[23]. In the field of building materials, application research is relatively abundant, with related journal publications ranking second in quantity[22]. Bayer process

ISSN: 2414-1895 DOI: 10.6919/ICJE.202604_12(4).0053

red mud is rich in aluminum mineral phases, making it an ideal carrier for chloride binding. The aluminum phases can be converted to Friedel's salt to efficiently immobilize Cl^-[26]. However, the direct utilization of Bayer process red mud faces two major challenges: its high alkali content easily causes concrete efflorescence and expansion cracking and the high content of inert mineral phases results in poor cementitious activity[27, 28]. Therefore, targeted treatment of these two issues is required before utilization.

Similar to industrial solid waste, the emission of industrial waste gases has also become a focus of attention in environmental protection. Global CO_2 annual emissions exceed 36 billion tons and continue to rise[29]. Existing research shows that carbonation treatment of industrial solid waste using acidic gases from industrial waste gases can improve their cementitious activity and enhance its performance[30]. Through the room-temperature in-situ wet carbonation activation of sintering process red mud, its CO_2 absorption can reach 15.3%, with significant improvements in compressive and flexural strength[31]. Wet carbonation of sintering process red mud enhances chloride binding capacity by promoting aluminum ion dissolution and enhancing Friedel's salt (FS) formation[26]. This wet carbonation process transforms red mud into a high-performance Cl^- binding agent through a three-in-one reaction of "dealkalization-carbon fixation-activation".

However, there are limited durability studies on wet carbonated Bayer red mud as a supplementary cementitious material. This paper aims to investigate the effect of different dosages of wet carbonated Bayer red mud (CBRM) on the chloride binding capacity of ordinary Portland cement (OPC). Given that chloride binding is influenced by multiple factors, this study designed composite salt conditions to evaluate the chloride binding performance of the composite cementitious material system containing Bayer red mud under such environments. Through analysis of hydration products and chloride binding performance, the variation patterns of chemical binding and physical adsorption can be inferred. This research not only helps to address the disposal challenge of aluminum industry solid waste and reduce environmental pollution, but also paves a new way for developing eco-friendly building materials and advancing global efforts towards carbon neutrality.

2. Experimental Programs

2.1 Materials

The ordinary Portland cement used in the experiment was supplied by Jiaozuo Qianye Cement Co. Ltd. The Bayer red mud (BRM) used was obtained from Chalco Zhongzhou Aluminum Co. Ltd. The Bayer red mud was subjected to dealkalization pretreatment through wet carbonation to enhance its cementitious activity[31], and was designated as carbonated (CBRM). The silver nitrate, sulfuric acid, calcium carbonate, and anhydrous ethanol used were all purchased from Tianjin Kemio Chemical Reagent Co. Ltd. Sodium chloride, calcium chloride, magnesium chloride hexahydrate, anhydrous sodium sulfate, and anhydrous magnesium sulfate produced by Tianjin Hedong Hongyan Reagent Factory were used. The particle size of all raw materials used was less than 200 mesh. X-ray fluorescence (XRF) analysis was employed to determine the chemical composition of cement, Bayer red mud, and carbonated Bayer red mud, as shown in Table 1. X-ray diffraction (XRD) analysis was employed to determine the mineral composition of cement, BRM and CBRM, as shown in Fig. 1, Fig. 2 and Fig. 3, respectively.

Table 1. Chemical composition of experimental raw materials (%)

Oxide	SiO_2	Al_2O_3	Fe_2O_3	CaO	MgO	SO_3	Na_2O	K_2O	LOI.
OPC	18.47	5.76	3.95	62.42	3.69	3.16	0.497	1.00	1.053
BRM	15.80	28.10	10.10	13.00	0.76	1.16	13.20	2.17	15.71
CBRM	19.45	24.69	11.99	13.85	1.22	1.03	8.59	0.90	18.28

ISSN: 2414-1895 DOI: 10.6919/ICJE.202604_12(4).0053

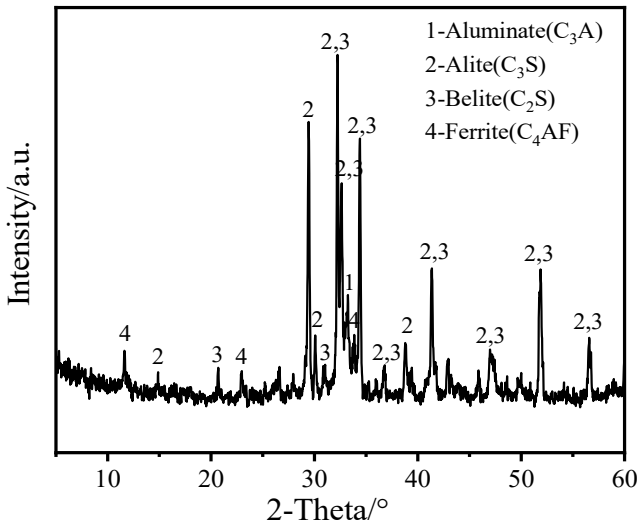

Fig. 1 XRD pattern of cement

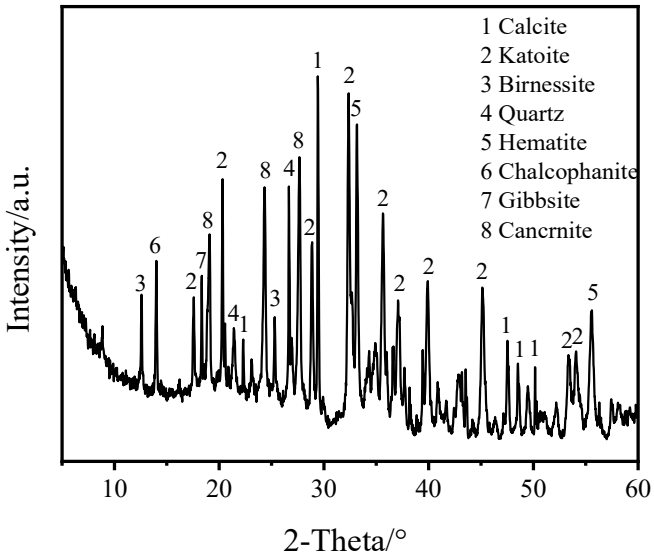

Fig. 2 XRD pattern of Bayer red mud

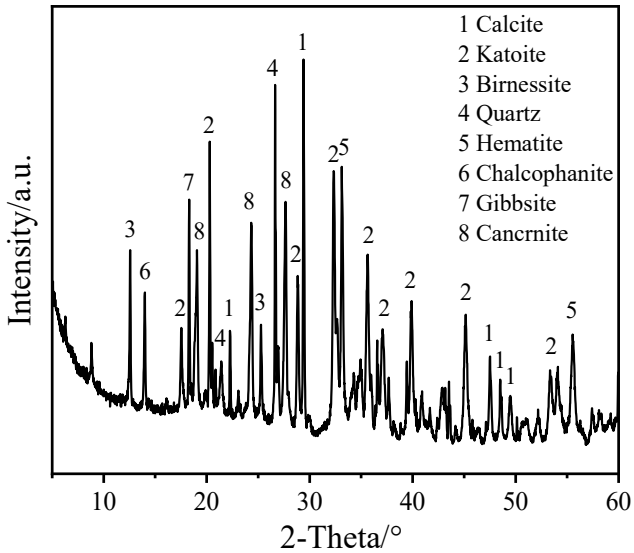

Fig. 3 XRD pattern of carbonated Bayer red mud

ISSN: 2414-1895 DOI: 10.6919/ICJE.202604_12(4).0053

2.2 Preparation of Hardened Cement Paste

CO_2 with a concentration of 99% was bubbled into conical flasks containing red mud slurry at a liquid-to-solid ratio of 10:1. Wet carbonation was carried out for 4 hours at a flow rate of 0.3 L/min under ambient temperature and pressure conditions. Subsequently, the filtrate was separated using a vacuum filtration pump to obtain carbonated CBRM for standby use. CBRM was used as a supplementary cementitious material to partially replace ordinary Portland cement (OPC), and the resulting composite cementitious system was designated as the OPC-CBRM system. Cement (OPC) and carbonated Bayer red mud (CBRM) were uniformly mixed according to the proportions shown in Table 2, and designated as CBRM0, CBRM10, CBRM20, CBRM30, CBRM40, and CBRM50, respectively. To ensure the mobility of the composite cementitious system, a water-to-binder ratio of 0.5 was used, and specimens were cured for 28 days in a standard curing room. The specimens cured to the designated age were crushed and sieved through 1.18 mm and 0.3 mm sieves, respectively. Particles with sizes between 0.3 mm and 1.18 mm were collected. The collected particles were mixed uniformly and immersed in anhydrous ethanol for 72 hours to terminate hydration. The anhydrous ethanol-treated particles were then dried in a vacuum oven for 24 hours and kept for standby use.

Table 2. Mix proportions of cement-carbonated Bayer red mud composite cementitious system

NO.	Cement(%)	CBRM(%)	w/b
CBRM0	100	0	0.5
CBRM10	90	10	0.5
CBRM20	80	20	0.5
CBRM30	70	30	0.5
CBRM40	60	40	0.5
CBRM50	50	50	0.5

2.3 Preparation of Salt Solution

Different amounts of analytical-grade sodium chloride reagent were dissolved in 100 mL of deionized water, respectively, and magnetically stirred in a water bath for 2 hours to prepare sodium chloride solutions of different concentrations[15]. Other different salt solutions were prepared using the same experimental method. The salt solution combination design is shown in Table 3.

Table 3. Design and designation of aggressive solution combinations

Abbreviation	Concentration of exposed solutions	Chloride ion（mol/L）
0.1NC	0.1mol/L NaCl	0.1
0.5NC	0.5mol/L NaCl	0.5
1.0NC	1.0mol/L NaCl	1.0
1.5NC	1.5mol/L NaCl	1.5
2.0NC	2.0mol/L NaCl	2.0
0.25CC	0.25mol/L $CaCl_2$	0.5
0.25MC	0.25mol/L $MgCl_2$	0.5
0.5NC-0.5NS	0.5mol/L NaCl+0.5mol/L Na_2SO_4	0.5
0.5NC-0.5MS	0.5mol/L NaCl+0.5mol/L $MgSO_4$	0.5

ISSN: 2414-1895 DOI: 10.6919/ICJE.202604_12(4).0053

2.4 Chloride Ion Binding Test

The dried particles were immersed in the prepared solutions (placed in the corresponding composite salt solutions according to different experimental purposes) for 7 days. Tang et al[32]. found that the concentration of the aggressive solution and the pore solution in the particles reached dynamic equilibrium after 7 days. The supernatant from the first immersion of particles was removed, designated as the first equilibrium solution, with volume recorded as V'. Subsequently, 200 ml of saturated lime water was added to the conical flask containing the first immersion particles, sealed and stored for 7 days. After 7 days, the concentration of the aggressive solution and the pore solution in the particles reached dynamic equilibrium again. The supernatant from the second immersion was removed, designated as the second equilibrium solution, with volume recorded as V". The test solutions were titrated using an automatic chloride ion titrator. The experimental procedure was conducted according to Fig. 4.

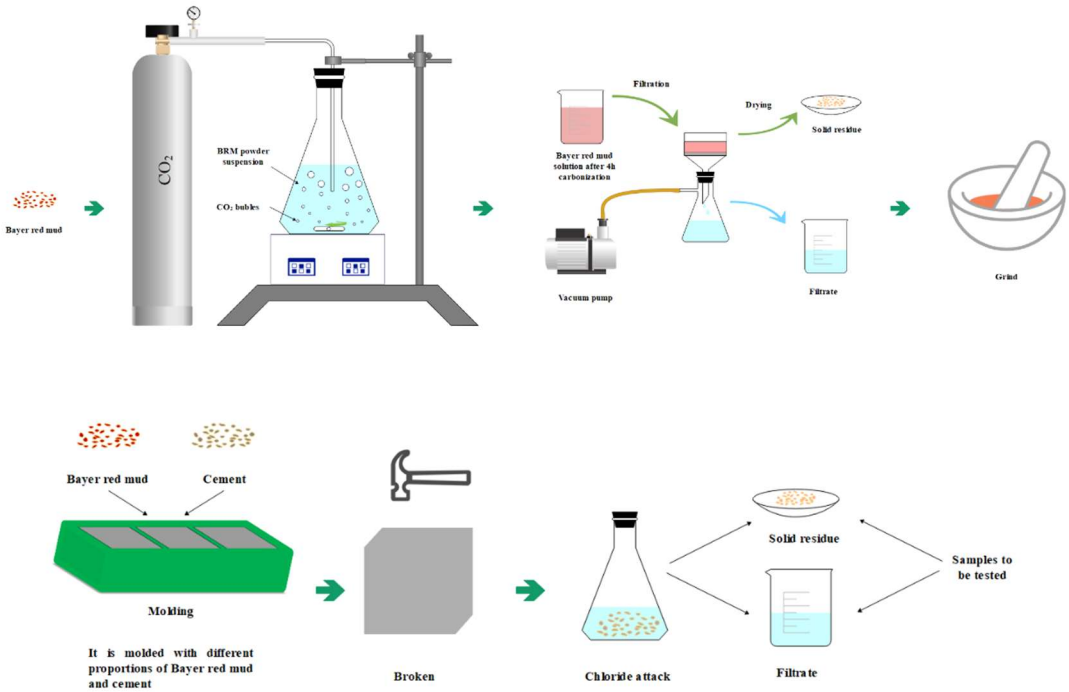

Fig. 4 Experimental flowchart

2.5 Test Methods

2.5.1. X-ray Diffractometer (XRD)

The test samples were ground using a three-head grinding mill, and it was ensured that the ground samples passed through a 200 mesh sieve. Mineral phase analysis was then conducted using X-ray diffraction with a scanning rate of 5°/min and a scanning range from 5° to 70°.

2.5.2. Thermogravimetric Analysis (TGA)

The test samples were ground using a three-head grinding mill, and it was ensured that the ground samples passed through a 200 mesh sieve. Sample testing was conducted using an HCT-3 computerized differential thermal balance manufactured by Beijing Hengjiu Scientific Instrument Factory. The test sample mass was approximately 15 mg, with a testing range of 40-1000 °C and a heating rate of 10 °C/min.

ISSN: 2414-1895 DOI: 10.6919/ICJE.202604_12(4).0053

2.5.3. Scanning Electron Microscopy (SEM)

The test samples were sieved using 0.45 mm and 0.90 mm sieves, and particles with sizes in the range of 0.45-0.90 mm were collected. After gold coating treatment under vacuum, the particle samples were observed for microstructural morphology using a MERLIN Compact scanning electron microscope manufactured by Carl Zeiss, Germany. The surface microstructural morphology of the samples was characterized under a working voltage of 10 kV.

2.5.4 Compressive Strength

The compressive strength of the samples was determined using a computer-controlled automatic compression testing machine (TYE-300B) with a loading rate of 0.1 kN/s. The experimental results were taken as the average of six specimen test results.

3. Results and Discussion

3.1 Different Dosages of Carbonated Bayer Red Mud

Fig. 5 shows the bound chloride content of the OPC-CBRM system at different ages. At 3 days of age, as shown in Fig. 5 (a), the OPC-CBRM system exhibited the highest bound chloride content when the CBRM dosage was 40%. Compared to the OPC system, the OPC-CBRM system showed increases of 59%, 80%, and 10% in total bound chloride content, chemically bound chloride content, and physically adsorbed chloride content, respectively. The increase in chemically bound chloride content was almost 8 times that of the increase in physically bound chloride content.

However, as shown in Fig. 5 (b), compared to the 3 days value, the bound chloride content of the OPC-CBRM system at 28 days decreased.Moreover, it can be clearly observed that the physically bound chloride content of the OPC-CBRM system was consistently lower than that of neat OPC paste, and exhibited a declining trend with increasing CBRM dosage.

At 28 days, the OPC-CBRM system with 30% incorporation increased the total and chemically bound chloride contents by 40% and 68%, respectively, compared to neat OPC. In contrast, the physically bound chloride content decreased by 12%. In summary, the incorporation of CBRM significantly improves the chloride binding capacity of cementitious materials, predominantly through enhanced chemical binding. Specifically, at 28 days, a 30% dosage proved optimal, yielding a 40% increase in total bound chloride content relative to the reference system.

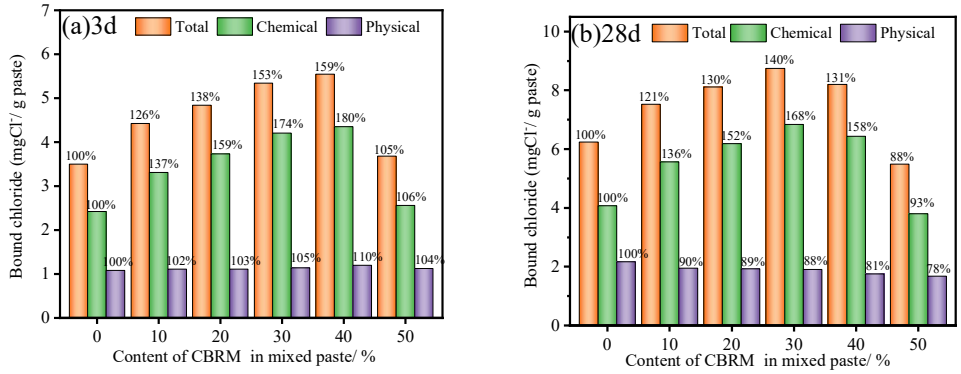

Fig. 5 Bound chloride content of OPC-CBRM system at different ages (a)3d, (b)28 d

Fig. 6 shows the XRD patterns of the OPC-CBRM system at different ages. It can be clearly observed from the figure that the variation patterns of diffraction peak intensities for various phases at 3 days and 28 days of age are essentially similar. The difference is that at 28 days of age, the diffraction peak intensity of FS begins to weaken when the CBRM dosage increases to 30%. This is consistent with the data analysis of the measured bound chloride content.

ISSN: 2414-1895 DOI: 10.6919/ICJE.202604_12(4).0053

When the CBRM dosage does not exceed 30%, the peak intensity corresponding to the FS diffraction peak increases with increasing carbonated Bayer red mud (CBRM) dosage. This is because the large amount of calcium carbonate contained in carbonated Bayer red mud (CBRM) forms monocarboaluminate during the hydration process, and under chloride attack, monocarboaluminate converts to FS, thus increasing the FS content[10, 33]. However, some scholars also believe that this is due to the large amount of aluminum oxide contained in carbonated Bayer red mud (CBRM), which increases the aluminum dissolution in the liquid phase, leading to a secondary pozzolanic effect that generates aluminates and further produces more FS[8, 34-36].

As the CBRM dosage increases, the calcite content increases correspondingly. This stems from two factors: first, CBRM itself contains calcite components; second, when C_3A is not completely reacted, the remaining calcium ions react with carbonate ions to form calcite (Cc). However, at 50% dosage, the calcite content significantly decreased, which may be attributed to the reaction between calcite and the hydration products of C_4AF[37, 38].

When the carbonated Bayer red mud (CBRM) dosage reached 50%, the peak intensity corresponding to FS showed a significant decrease. This is influenced by two factors: first, CBRM incorporation dilutes the OPC components, directly reducing FS formation; second, the pozzolanic reaction continuously consumes CH, leading to a decrease in CH content in the cementitious materials. Since carbonated Bayer red mud (CBRM) hydration requires CH, the reduction of CH leads to incomplete hydration, further inhibiting FS formation[39]. Moreover, the diffraction peak of gibbsite (Gib) becomes very strong. This indicates that the hydration reactions in the OPC-CBRM composite system are essentially complete, and aluminum oxide exists predominantly as hydroxide in the form of Gib.

In summary, when the CBRM dosage is 30%, the OPC-CBRM system exhibits the strongest chloride binding capacity. This is consistent with the measured bound chloride content of the OPC-CBRM system.

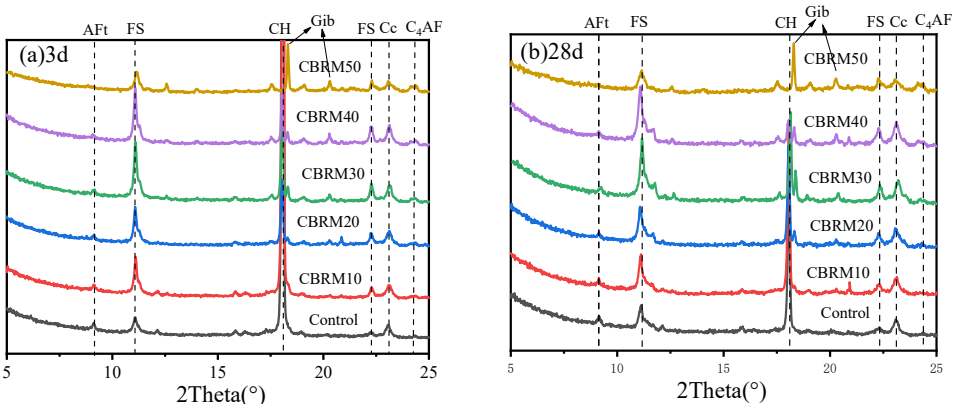

Fig. 6 XRD patterns of OPC-CBRM system at different ages (a)3d , (b) 28d

Fig. 7 shows the DTG spectra of cement with 30% CBRM incorporation at different ages. From the characteristics of DTG curve changes in Fig. 7, it can be observed that regardless of whether at 3 days or 28 days, the FS peaks in the OPC-CBRM system are sharper than those in neat cement paste, indicating that carbonated Bayer red mud (CBRM) incorporation can promote the formation of more FS in cementitious materials. Additionally, it can be clearly observed from Fig. 7 that the peaks for AFt and C-S-H in the OPC-CBRM system are both smaller, and these two phases are the main factors for physical adsorption, which is consistent with the data analysis results of physical adsorption. Furthermore, due to the significant overlap between the dehydration peak range of Gib and the dehydroxylation peak range of FS at 200-380°C, thermogravimetric analysis may not be able to accurately quantify the variation patterns of the FS phase[26].

ISSN: 2414-1895 DOI: 10.6919/ICJE.202604_12(4).0053

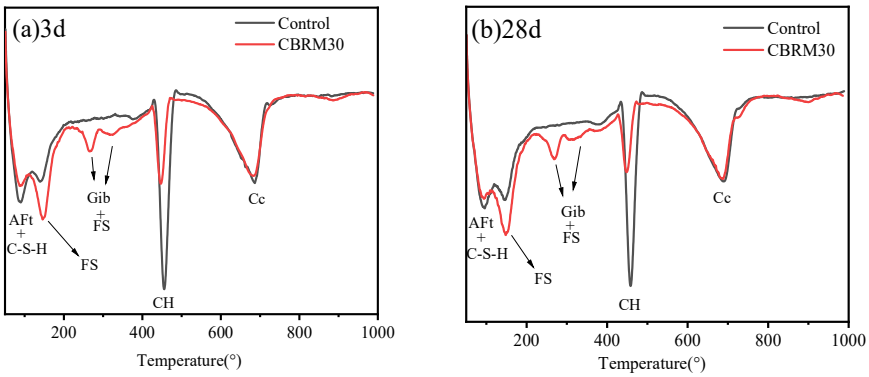

Fig. 7 DTG curves of OPC-CBRM system at different ages (a) 3d, (b) 28d

Fig. 8 shows the SEM images of OPC and OPC-CBRM system (OPC-CBRM30) after 3 days of hydration. It can be clearly observed from the figure that at 3 days of age, a large amount of C-S-H gel and AFt were observed in neat cement paste, but Friedel's salt (FS) was not observed. This may be because at 3 days of age, the formation of FS in neat cement paste is relatively limited and is masked by C-S-H gel and AFt. Compared to neat cement paste, distinct FS, C-S-H gel, and AFt were observed in the OPC-CBRM system. It can be seen that CBRM incorporation can promote the formation of more FS in cementitious materials. However, the dilution effect of CBRM on cement leads to a reduction in the formation of C-S-H gel and AFt in the OPC-CBRM paste.

Fig. 9 shows the SEM images of OPC and OPC-CBRM system (CBRM30) after 28 days of hydration. It can be clearly observed from the figure that at 28 days of age, a large amount of C-S-H gel, AFt, and a small amount of FS were observed in neat cement paste. In the OPC-CBRM system, distinct FS, a small amount of C-S-H gel and AFt were observed, with changes similar to those at 3 days of age. In summary, CBRM incorporation can promote the formation of more FS in cementitious materials. This is consistent with the analysis results from XRD and TG-DTG.

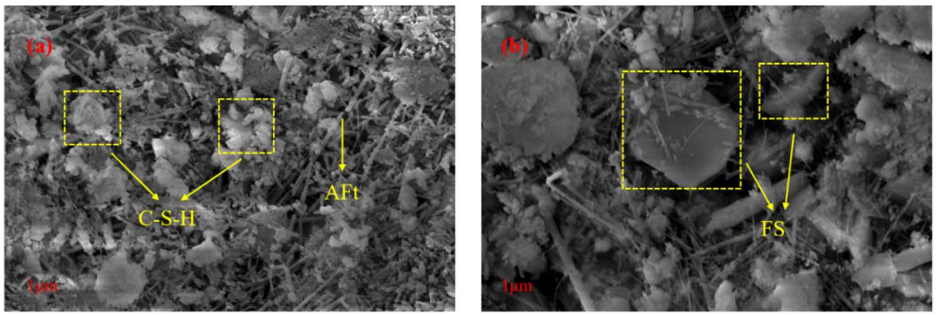

Fig. 8 SEM images of cement hydrated and hardened for 3 days (a) OPC, (b) OPC-CBRM (CBRM30)

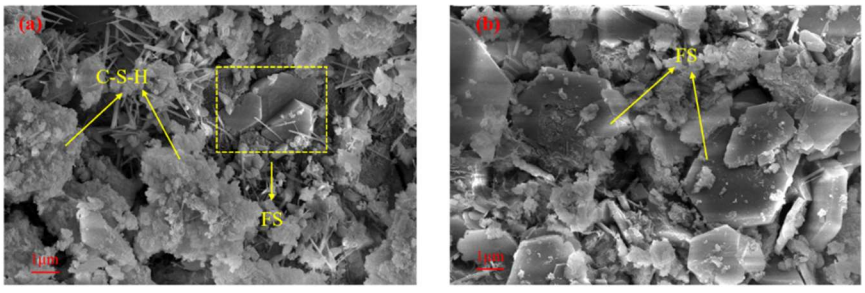

Fig. 9 SEM images of cement hydrated and hardened for 28 days (a) OPC, (b) OPC-CBRM (CBRM30)

ISSN: 2414-1895 DOI: 10.6919/ICJE.202604_12(4).0053

3.2 Isotherm

Fig. 10 shows the influence curves of chloride binding capacity of cement blended with 30% CBRM under different curing ages and chloride ion concentration conditions. In this study, Langmuir and Freundlich adsorption isotherms were employed to fit the relationship between free chloride ions and bound chloride ions within the concentration range of 0.0-2.0 mol/L. Langmuir adsorption isotherms are generally applicable for fitting at relatively low free chloride concentrations (< 0.05 mol/L), while Freundlich adsorption isotherms are suitable for higher free chloride concentrations (> 0.05 mol/L)[32]. The expressions for Langmuir and Freundlich adsorption isotherms are as follows[40]:

Langmuir isotherm: $C_b = a \times C_f/(1 + b \times C_f)$

Freundlich isotherm: $C_b = a \times C_f^b$

where a and b are binding constants.

From Fig. 10, it can be clearly observed that the bound chloride content in the OPC-CBRM system increases with the increase of chloride ion concentration in the aggressive solution across all curing ages.

Table **4** presents the fitting parameters a and b, and correlation coefficients R^2 for Freundlich and Langmuir fitting of the OPC-CBRM system. From

Table **4**, it can be seen that the average correlation coefficients (R^2) for Freundlich and Langmuir fitting of the OPC-CBRM system are 0.9882 and 0. 9270, respectively. For fitting at different curing ages as well as the average values, the Freundlich fitting performance is more satisfactory than that of the Langmuir fitting, which is consistent with the conclusions of previous researchers[41, 42].

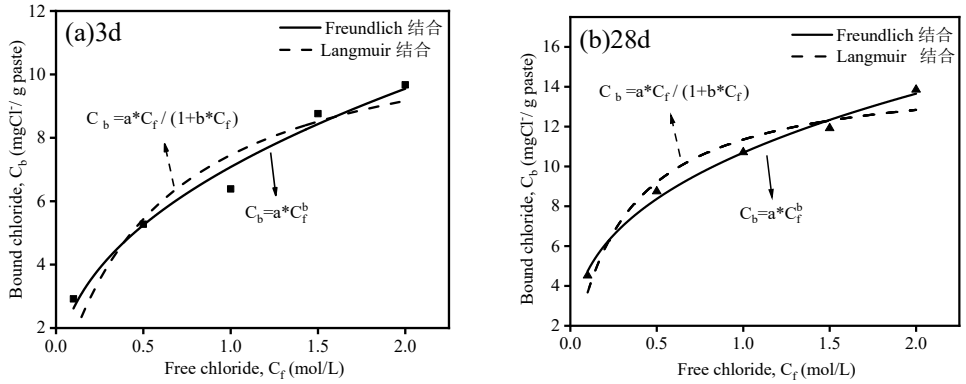

Fig. 10 Bound chloride curves of OPC-CBRM system at different ages (a)3d, (b)28d

Table 4. Isotherm fitting parameters and correlation coefficients for OPC-CBRM system

	Freundlich combination			Langmuir combination		
	a	b	R^2	a	b	R^2
3d	7.13	0.43	0.9855	20.67	1.75	0.9146
28d	10.69	0.35	0.9920	48.88	3.31	0.9503
Average	-	-	0.9882	-	-	0.9270

From Fig. 11, it can be clearly observed that when the Cl^- concentration in the aggressive solution is 0.1 mol/L, the diffraction peaks of FS in the OPC-CBRM system are very weak, with KS diffraction peaks present; when the Cl^- concentration in the aggressive solution exceeds 0.1 mol/L, the KS diffraction peaks in the OPC-CBRM system disappear, while the FS diffraction peaks become stronger with very distinct changes. This indicates that KS in the paste is formed under low Cl^-

ISSN: 2414-1895 DOI: 10.6919/ICJE.202604_12(4).0053

concentrations (<0.5 mol/L); when the Cl^- concentration in the aggressive solution increases (>0.5 mol/L), KS transforms to FS[43]. Additionally, it can be clearly observed from the figure that the diffraction peaks of FS and Cc first increase and then decrease with the increase of chloride ion concentration in the aggressive solution. When the Cl^- concentration in the aggressive solution is 0.5 mol/L, AFt is produced in small amounts, and both CH content and FS content reach their maximum values. This is mainly because CH can maintain the high alkaline environment of the system, thereby promoting the formation of FS[44].

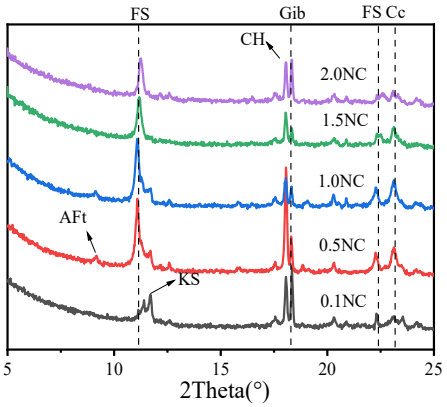

Fig. 11 XRD patterns of OPC-CBRM system hydrated for 28 days under attack by different concentrations of sodium chloride solutions

3.3 Metal Cations

Fig. 12 shows the bound chloride content of the OPC-CBRM system under different curing ages and different chloride salt types. From the figure, it can be clearly observed that the composite system immersed in calcium chloride aggressive solution exhibits the highest bound chloride content, followed by the composite system immersed in magnesium chloride aggressive solution, and finally the composite system immersed in sodium chloride aggressive solution. This indicates that both Ca^{2+} and Mg^{2+} can promote chloride binding in the OPC-CBRM composite system, and the longer the curing age, the greater the increase in bound chloride content of the OPC-CBRM system. Additionally, compared with the composite system immersed in magnesium chloride aggressive solution, the composite system immersed in calcium chloride aggressive solution shows a greater increase in bound chloride content. This is because C-S-H and $Ca(OH)_2$ bind more chloride ions than magnesium silicate hydrate (M-S-H) and $Mg(OH)_2$, therefore calcium chloride aggressive solution contains more bound chloride ions and total chloride ions than magnesium chloride aggressive solution[45, 46].

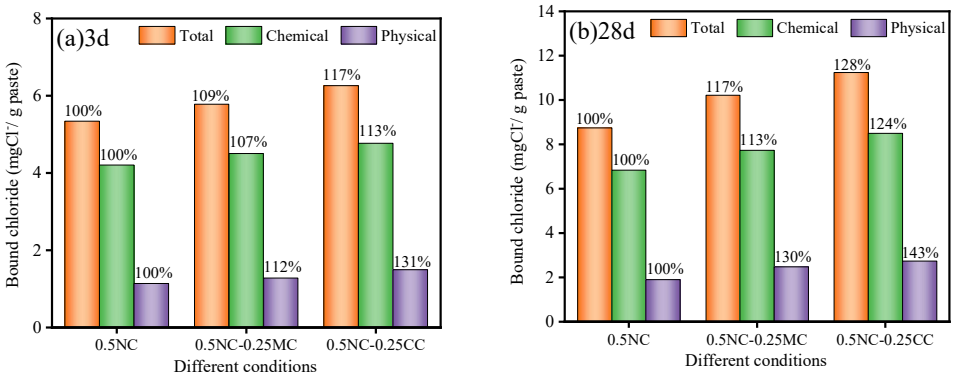

Fig. 12 Bound chloride content of OPC-CBRM system under attack by different chloride solutions at different ages (a)3d, (b)28d

ISSN: 2414-1895 DOI: 10.6919/ICJE.202604_12(4).0053

Fig. 13 shows the XRD patterns of the OPC-CBRM system hydrated for 28 days under aggressive exposure to different cations and different chloride salt solutions. From the figure, it can be observed that under $MgCl_2$ and $CaCl_2$ aggressive environments, there are no AFt diffraction peaks in the OPC-CBRM system. It is speculated that the presence of Mg^{2+} and Ca^{2+} promotes the ion exchange reaction between Cl^- in the aggressive solution and AFt, forming FS and thus causing the disappearance of AFt[47]. Additionally, under $MgCl_2$ aggressive environment, no CH diffraction peaks are observed in the OPC-CBRM system. This is because the presence of Mg^{2+} causes the dissolution of $Ca(OH)_2$ in the OPC-CBRM system, thus leading to the disappearance of CH diffraction peaks[48].

Furthermore, it can be clearly observed from Fig. 14 that the paste immersed in calcium chloride aggressive solution exhibits the strongest FS diffraction peaks, indicating that Ca^{2+} promotes the formation of more FS in the OPC-CBRM system. In summary, it can be concluded that the presence of Mg^{2+} and Ca^{2+} can enhance the chloride binding capacity of the OPC-CBRM composite cementitious system, with the influence order being $Ca^{2+} > Mg^{2+} > Na^+$.

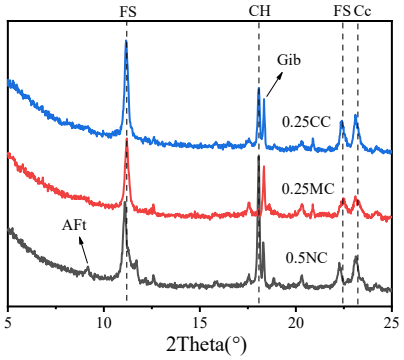

Fig. 13 XRD patterns of OPC-CBRM system hydrated for 28 days under attack by different chloride solutions

3.4 Sulfate Concentration

Fig. 14 shows the bound chloride content of the OPC-CBRM system under sulfate attack at different curing ages and different concentrations. From the figure, it can be clearly observed that after introducing SO_4^{2-} into the NaCl aggressive solution, the total bound chloride, chemically bound chloride, and physically bound chloride of the composite cementitious system all show significant decreases, with the reduction increasing as the SO_4^{2-} concentration rises. Specifically, the presence of sulfate significantly reduced the chloride binding capacity of the OPC-CBRM system. At 3 days, the bound chloride contents decreased by approximately 38%–57% depending on the sulfate concentration. This inhibitory effect became more pronounced at 28 days, where the reductSions ranged from 50% to 65%, peaking at 1.0 mol/L SO_4^{2-} concentration.

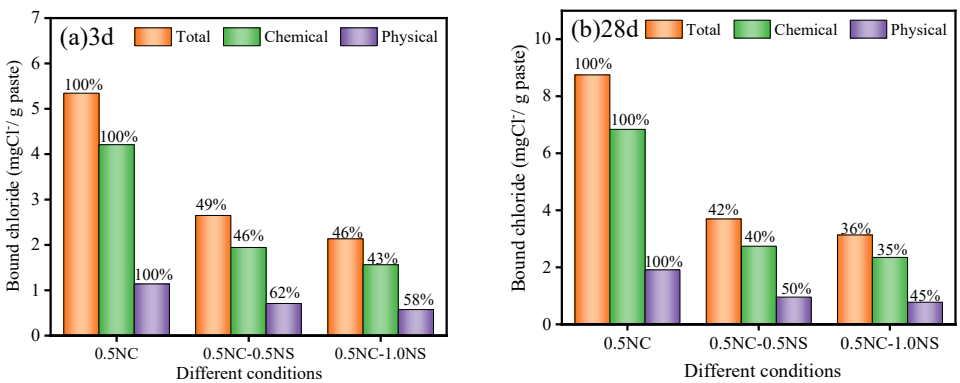

Fig. 14 Bound chloride content of OPC-CBRM system under attack by different concentrations of sulfate solutions at different ages (a)3d, (b)28d

ISSN: 2414-1895 DOI: 10.6919/ICJE.202604_12(4).0053

Specifically, the presence of SO_4^{2-} in the aggressive solution significantly compromised the chloride binding capacity of the OPC-CBRM system. At 3 days, the bound chloride contents decreased by approximately 38%–57% depending on the sulfate concentration (0.5–1.0 mol/L). Notably, this inhibitory effect became more pronounced at the later curing stage (28 days), where the reductions further expanded to 50%–65%. In summary, SO_4^{2-} is detrimental to chloride binding in the composite system, and this adverse effect intensifies with both higher sulfate concentrations and longer curing ages.

(2) XRD analysis

Fig. 15 shows the XRD patterns of the OPC-CBRM system hydrated for 28 days under attack by sulfate solutions of different concentrations. In the NaCl aggressive environment, the main phases in the OPC-CBRM system are: ettringite (AFt), calcium hydroxide (CH), Friedel's salt (FS), gibbsite (Gib), and calcite (Cc); after introducing SO_4^{2-} into the NaCl aggressive environment, the main phases in the OPC-CBRM system are: Friedel's salt (FS), gibbsite (Gib), gypsum (Gyp), and calcite (Cc). It can be found that after introducing SO_4^{2-} into the NaCl aggressive environment, the diffraction peaks of FS in the OPC-CBRM system show obvious weakening. This indicates that introducing SO_4^{2-} into the NaCl aggressive environment is detrimental to the formation of Friedel's salt. This is because SO_4^{2-} consumes the aluminate phases in cement components and cement hydration products, thereby reducing the formation of FS. It can also be clearly observed from Fig. 15 that the diffraction peaks of Gib intensify with the increase of SO_4^{2-} concentration in the aggressive solution, while the diffraction peaks of Cc weaken with the increase of SO_4^{2-} concentration in the aggressive solution[49]. Additionally, when low concentration sulfate ions are introduced, the sulfate ions react with the cement hydration product calcium hydroxide (CH) to form a small amount of gypsum, with the reaction formula being (3):

$$Ca(OH)_2 + SO_4^{2-} + 2H_2O \rightarrow CaSO_4\,2H_2O + 2OH^- \quad (3)$$

Studies have found[37, 50, 51] that after low-concentration sulfate attack, due to SO_4^{2-} replacing Cl^-, Friedel's salt transforms to AFm-SO_4, leading to desorption of chemically bound chloride, with the reaction formula being.

However, in high-concentration sulfate solutions, the thermodynamic stability of the AFt phase is higher than that of AFm-Cl (FS). According to the phase equilibrium principle, the system will spontaneously proceed toward the formation of the more stable phase (AFt), driving the decomposition of FS.

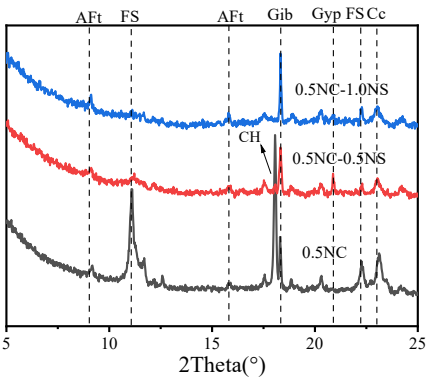

Fig. 15 XRD patterns of OPC-CBRM system hydrated for 28 days under attack by different concentrations of sulfate solutions

ISSN: 2414-1895 DOI: 10.6919/ICJE.202604_12(4).0053

In summary, the presence of SO_4^{2-} is detrimental to chloride binding in the OPC-CBRM system. There are two reasons: on one hand, the presence of SO_4^{2-} causes Ca^{2+} leaching from C-S-H gel, thereby reducing the physical adsorption capacity of C-S-H gel for chloride ions; on the other hand, after introducing SO_4^{2-} into the aggressive environment, SO_4^{2-} undergoes ion exchange reactions with Cl^- in Friedel's salt, leading to the decomposition of Friedel's salt and thus affecting the stability of chemically bound chloride ions.

3.5 Sulfate Type

Fig. 16 presents the bound chloride content of the OPC-CBRM system under different sulfate attacks. Clearly, the introduction of either Na_2SO_4 or $MgSO_4$ into the NaCl solution induced a substantial reduction (>50%) in total, chemically, and physically bound chloride contents. At the early stage (3 days), the impact of sulfate type was marginal. However, at 28 d, the reduction became significantly more pronounced. Furthermore, compared to the Na_2SO_4 group (0.5 NC - 0.5 NS), the specimens exposed to $MgSO_4$ (0.5 NC - 0.5 MS) exhibited a more severe loss in bound chloride content.

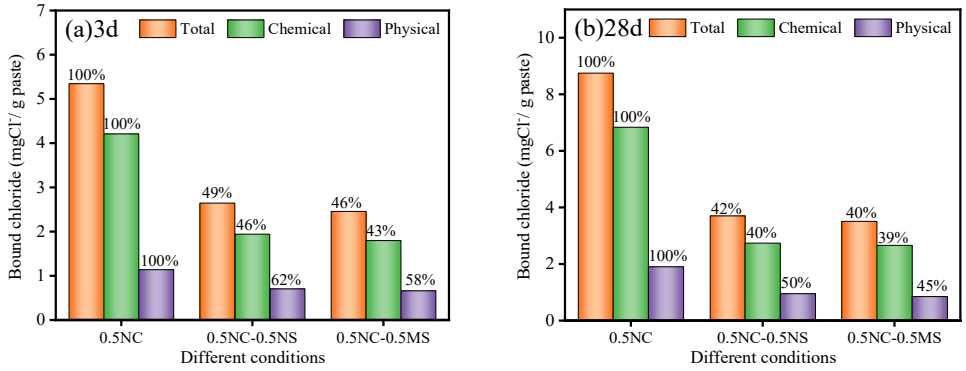

Fig. 16 Bound chloride content of OPC-CBRM system under attack by different sulfatesolutions at different ages (a)3d, (b)28d

Fig. 17 illustrates the XRD patterns of the OPC-CBRM system under different sulfate attacks. Compared to the NaCl reference, the mineralogical composition changed significantly in sulfate environments. The most notable alteration was the disappearance of $Ca(OH)_2$ and the simultaneous emergence of gypsum in both 0.5NS and 0.5MS solutions, indicating the consumption of portlandite by sulfate attack. Furthermore, regarding the chloride-binding phase, Friedel's salt remained stable in the Na_2SO_4 environment but was not detected in the $MgSO_4$ environment, suggesting its decomposition due to the attack of magnesium ions.

After introducing Na_2SO_4 into the NaCl aggressive solution, the diffraction peaks of CH in the OPC-CBRM system disappear, the diffraction peaks of FS show obvious weakening and almost disappear, while gypsum (Gyp) diffraction peaks appear but with low intensity; after introducing $MgSO_4$ into the NaCl aggressive solution, the diffraction peaks of both CH and FS in the OPC-CBRM system disappear, and distinct AFt diffraction peaks appear. This is because in the 0.5NC-0.5MS aggressive solution, Mg^{2+} reacts with hydroxide ions to form brucite, and the formation of brucite hinders the entry of Cl^- into the interior of cementitious materials, thereby leading to reduced FS formation. Moreover, compared with Na_2SO_4, $MgSO_4$ promotes the formation of more ettringite and gypsum in the OPC-CBRM system[38, 39, 50].

In summary, introducing Na_2SO_4 or $MgSO_4$ into NaCl aggressive solution is detrimental to chloride binding in the OPC-CBRM system. Moreover, compared with Na_2SO_4 attack, $MgSO_4$ attack has a greater detrimental effect on chloride binding in the OPC-CBRM system, and the longer the curing age, the greater the detrimental effects of Na_2SO_4 and $MgSO_4$ attack on chloride binding in the OPC-CBRM system.

ISSN: 2414-1895 DOI: 10.6919/ICJE.202604_12(4).0053

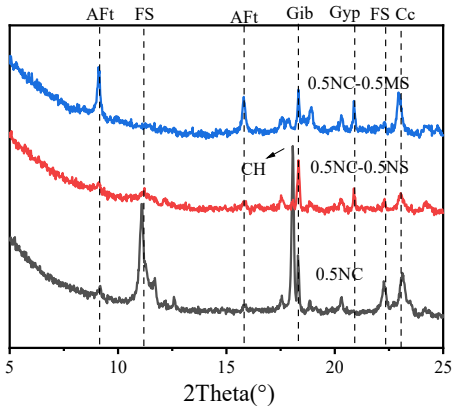

Fig. 17 XRD patterns of OPC-CBRM system hydrated for 28 days under attack by different types of sulfate solutions

3.6 Compressive Strength

As illustrated in Fig. 18, the compressive strength of the OPC-CBRM system exhibits a continuous decline with increasing CBRM dosage at both 3 and 28 days. Specifically, when the CBRM dosage increased from 10% to 50%, the strength at 3 days decreased by 10.2%, 16.3%, 22.0%, 32.1%, and 36.1%, respectively, compared to plain cement paste. Similarly, at 28 days, the reductions were 12.3%, 17.9%, 24.5%, 29.6%, and 34.2%, respectively. Interestingly, the magnitude of reduction varied with curing age: when the dosage was low (≤30%), the strength reduction at 3 days was lower than that at 28 days; conversely, when the dosage exceeded 30%, the reduction at 3 days became more severe than at 28 days.

The reasons for these phenomena are analyzed as follows. The overall strength reduction is primarily attributed to the dilution effect (reduced clinker content) and the high alkali content in CBRM, which may lead to a porous microstructure[52]. Regarding the variation at different ages, since C-S-H gel dominates cement strength[53], the lower reduction at the early stage with low dosage (≤30%) suggests that C-S-H gel formation is relatively favored at 3 days compared to 28 days. However, at high dosages (>30%), the calcium hydroxide (CH) produced by early hydration is insufficient to react with the excessive CBRM, thereby hindering early strength development and leading to a higher reduction at 3 days[54].

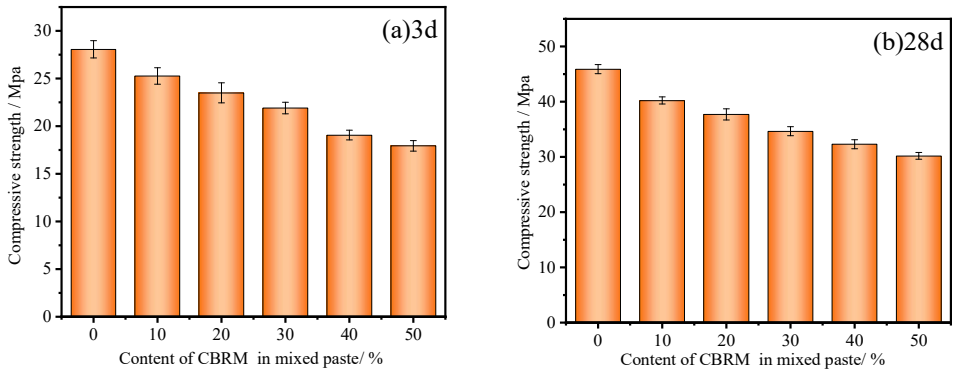

Fig. 18 Compressive strength of OPC-CBRM system at different ages (a) 3d, (b) 28d

4. Conclusion

This study systematically reveals the influence of CBRM as a supplementary cementitious material on the chloride binding capacity of cement-based materials. The main conclusions are as follows:

(1) CBRM promotes the formation of Friedel's salt (FS) through dual pathways: first, active aluminum ions released from carbonated red mud form aluminate precursors through secondary pozzolanic reactions; second, calcium carbonate ($CaCO_3$) in CBRM generates monocarboaluminate during

ISSN: 2414-1895 DOI: 10.6919/ICJE.202604_12(4).0053

hydration, and the interlayer $CaCO_3$ is subsequently replaced by chloride ions via ion exchange to form FS. When the CBRM dosage is 30%, the total and chemically bound chloride contents increased by 40% and 68%, respectively, compared to plain cement paste, while the physically adsorbed chloride decreased by 12% due to the reduction of C-S-H gel.

(2) The Freundlich model ($R^2 = 0.9882$) is more applicable to the CBRM system than the Langmuir model ($R^2 = 0.9270$), indicating that the adsorption process is dominated by heterogeneous interfaces. A critical threshold (0.5 mol/L) exists for chloride ion concentration: at low concentrations, the AFm phase exists in the form of Kuzel's salt (KS); when the concentration exceeds the threshold, KS gradually transforms to FS, and the FS diffraction peak intensity shows a trend of first increasing and then decreasing with increasing concentration.

(3) Ca^{2+} stabilizes the C-S-H double electric layer and enhances AFm phase affinity, resulting in 23% higher FS formation under $CaCl_2$ attack compared to $MgCl_2$; conversely, Mg^{2+} inhibits FS stability by dissolving calcium hydroxide (CH). SO_4^{2-} reduces total bound chloride content by 58% - 64% through competing for AFm interlayer sites and consuming calcium sources to form gypsum. $MgSO_4$ has a stronger negative impact than Na_2SO_4 due to the simultaneous introduction of both Mg^{2+} and SO_4^{2-}.

(4) Increasing CBRM dosage leads to a linear decrease in compressive strength, with 3 days and 28 days strengths reduced by 22% and 24.5% respectively at 30% dosage. The primary causes of strength loss are the reduction of C-S-H gel (dilution effect) and the porous microstructure induced by the high alkali content in CBRM. It is recommended to use CBRM in non-load-bearing structures for marine engineering applications, and compensate for strength deficiencies through blending with nanomaterials or optimizing curing regimes.

This study provides theoretical basis for red mud resource utilization and marine engineering durability enhancement, improving the utilization efficiency of both and reducing environmental pollution. Meanwhile, it improved the chloride binding capacity of cement-based materials, which helps to mitigate steel reinforcement corrosion, extend the service life of reinforced concrete structures, and has significant implications for marine engineering and other fields. Future research needs to further explore the synergistic effects of CBRM-industrial by-products and the evolution patterns of long-term service performance.

Credit Authorship Contribution Statement

Yujie Song: Writing – original draft, Software, Methodology, Investigation. Mifeng Gou: Writing – review & editing, Supervision, Resources. Yanze Xiong: Writing – review & editing, Investigation, Formal analysis. Jian Lu: Writing – review &editing, Investigation. Zhen Zhang: Writing – review & editing, Investigation. Hongxiao Chen: Writing – review & editing, Investigation. Mingyang Xu: Writing – review & editing, Investigation.

Declaration of Competing Interest

No conflict of interest exists in the submission of this manuscript, and the manuscript is approved by all authors for publication. We declare that the work described is original research that has not been published previously.

Data Availability

No data was used for the research described in the article.

Acknowledgments

This work was supported by the National Key R&D Program of China (2024YFF0508300)

ISSN: 2414-1895 DOI: 10.6919/ICJE.202604_12(4).0053

References

[1] D. Daneshvar, A. Behnood, A. Robisson, Interfacial bond in concrete-to-concrete composites: A review, Construction and Building Materials 359 (2022) 129195.

[2] G. Habert, S.A. Miller, V.M. John, J.L. Provis, A. Favier, A. Horvath, K.L. Scrivener, Environmental impacts and decarbonization strategies in the cement and concrete industries, Nature Reviews Earth & Environment 1(11) (2020) 559-573.

[3] H. Qin, S. Ding, A. Ashour, Q. Zheng, B. Han, Revolutionizing infrastructure: The evolving landscape of electricity-based multifunctional concrete from concept to practice, Progress in Materials Science 145 (2024).

[4] Y. Cao, C. Gehlen, U. Angst, L. Wang, Z. Wang, Y. Yao, Critical chloride content in reinforced concrete - An updated review considering Chinese experience, Cement and Concrete Research 117 (2019) 58-68.

[5] T. Senga Kiesse, S. Bonnet, O. Amiri, A. Ventura, Analysis of corrosion risk due to chloride diffusion for concrete structures in marine environment, Marine Structures 73 (2020) 102804.

[6] X. Hu, C. Shi, Q. Yuan, J. Zhang, G. De Schutter, Changes of pore structure and chloride content in cement pastes after pore solution expression, Cement and Concrete Composites 106 (2020) 103465.

[7] T.U. Mohammed, H. Hamada, Relationship between free chloride and total chloride contents in concrete, Cement and Concrete Research 33(9) (2003) 1487-1490.

[8] Z. Shi, M.R. Geiker, K. De Weerdt, T.A. Østnor, B. Lothenbach, F. Winnefeld, J. Skibsted, Role of calcium on chloride binding in hydrated Portland cement–metakaolin–limestone blends, Cement and Concrete Research 95 (2017) 205-216.

[9] I. Galan, F.P. Glasser, Chloride in cement, Advances in Cement Research 27(2) (2015) 63-97.

[10] Z. Lv, H. Tan, X. Liu, P. Chen, Y. Wang, W. Liang, J. Hong, Chloride binding of AFm in the presence of Na+, Ca2+ and Ba2+, Construction and Building Materials 364 (2023) 129804.

[11] S. Pourchet, L. Regnaud, J.P. Perez, A. Nonat, Early C3A hydration in the presence of different kinds of calcium sulfate, Cement and Concrete Research 39(11) (2009) 989-996.

[12] A. Mesbah, M. François, C. Cau-dit-Coumes, F. Frizon, Y. Filinchuk, F. Leroux, J. Ravaux, G. Renaudin, Crystal structure of Kuzel's salt 3CaO·Al2O3·1/2CaSO4·1/2CaCl2·11H2O determined by synchrotron powder diffraction, Cement and Concrete Research 41(5) (2011) 504-509.

[13] H. He, H. Qiao, T. Sun, H. Yang, C. He, Research progress in mechanisms, influence factors and improvement routes of chloride binding for cement composites, Journal of Building Engineering 86 (2024) 108978.

[14] Y. Elakneswaran, A. Iwasa, T. Nawa, T. Sato, K. Kurumisawa, Ion-cement hydrate interactions govern multi-ionic transport model for cementitious materials, Cement and Concrete Research 40(12) (2010) 1756-1765.

[15] F. Georget, C. Bénier, W. Wilson, K.L. Scrivener, Chloride sorption by C-S-H quantified by SEM-EDX image analysis, Cement and Concrete Research 152 (2022) 106656.

[16] F. Wu, H. Bi, H. Lin, X. Wang, C. Luan, X. Cheng, S. Wang, Y. Huang, Physical and chemical chloride binding characteristics of the hydration products for phosphoaluminate cement, Construction and Building Materials 403 (2023) 133044.

[17] B. Martín-Pérez, H. Zibara, R.D. Hooton, M.D.A. Thomas, A study of the effect of chloride binding on service life predictions, Cement and Concrete Research 30(8) (2000) 1215-1223.

[18] L.B. Yu, L.H. Jiang, H.Q. Chu, M.Z. Guo, Z.Y. Zhu, H. Dong, Effect of electrochemical chloride removal and ground granulated blast furnace slag on the chloride binding of cement paste subjected to NaCl and Na2SO4 attack, Construction and Building Materials 220 (2019) 538-546.

[19] X. Chen, Y. He, L. Lu, F. Wang, S. Hu, Effects of curing regimes on the chloride binding capacity of cementitious materials, Construction and Building Materials 342 (2022).

[20] P. Chen, B. Ma, H. Tan, X. Liu, T. Zhang, C. Li, Q. Yang, Z. Luo, Utilization of barium slag to improve chloride-binding ability of cement-based material, Journal of Cleaner Production 283 (2021).

ISSN: 2414-1895 DOI: 10.6919/ICJE.202604_12(4).0053

[21] Y. Guo, T. Zhang, W. Tian, J. Wei, Q. Yu, Physically and chemically bound chlorides in hydrated cement pastes: a comparison study of the effects of silica fume and metakaolin, Journal of Materials Science 54(3) (2018) 2152-2169.

[22] A. Niu, C. Lin, Trends in research on characterization, treatment and valorization of hazardous red mud: A systematic review, Journal of Environmental Management 351 (2024).

[23] S. Wang, H. Jin, Y. Deng, Y. Xiao, Comprehensive utilization status of red mud in China: A critical review, Journal of Cleaner Production 289 (2021).

[24] W. Liu, X. Chen, W. Li, Y. Yu, K. Yan, Environmental assessment, management and utilization of red mud in China, Journal of Cleaner Production 84 (2014) 606-610.

[25] M. Jovičević-Klug, I.R. Souza Filho, H. Springer, C. Adam, D. Raabe, Green steel from red mud through climate-neutral hydrogen plasma reduction, Nature 625(7996) (2024) 703-709.

[26] M. Gou, M. Zhang, X. Yang, S. Liu, X. Hou, J. Ji, Valorization of industrial wastes for sustainable cement-based materials with enhanced chloride binding, Journal of Building Engineering 95 (2024).

[27] X. Zhou, Z. Geng, J. Shi, Enhanced passivity of reinforcing steel in cementitious materials with thermally-activated red mud, Cement and Concrete Composites 153 (2024).

[28] R. Snellings, P. Suraneni, J. Skibsted, Future and emerging supplementary cementitious materials, Cement and Concrete Research 171 (2023).

[29] F. Nocito, A. Dibenedetto, Atmospheric CO2 mitigation technologies: carbon capture utilization and storage, Current Opinion in Green and Sustainable Chemistry 21 (2020) 34-43.

[30] S. Liu, C. Pan, H. Zhang, S. Yao, P. Shen, X. Guan, C. Shi, H. Li, Development of novel mineral admixtures for sulphoaluminate cement clinker: The effects of wet carbonation activated red mud, Journal of Building Engineering 67 (2023).

[31] S. Liu, Y. Shen, Y. Wang, P. Shen, D. Xuan, X. Guan, C. Shi, Upcycling sintering red mud waste for novel superfine composite mineral admixture and CO2 sequestration, Cement and Concrete Composites 129 (2022).

[32] T. Luping, L.-O. Nilsson, Chloride binding capacity and binding isotherms of OPC pastes and mortars, Cement and Concrete Research 23(2) (1993) 247-253.

[33] I.G. Richardson, Tobermorite/jennite- and tobermorite/calcium hydroxide-based models for the structure of C-S-H: applicability to hardened pastes of tricalcium silicate, β-dicalcium silicate, Portland cement, and blends of Portland cement with blast-furnace slag, metakaolin, or silica fume, Cement and Concrete Research 34(9) (2004) 1733-1777.

[34] B. Díaz, L. Freire, X.R. Nóvoa, M.C. Pérez, Chloride and CO2 transport in cement paste containing red mud, Cement and Concrete Composites 62 (2015) 178-186.

[35] X. Fan, Y. Wang, Q. Yu, X. Gao, J. Ye, Y. Zhang, Improving the chloride binding capacity of alkali activated slag by calcium and aluminum enriched minerals, Journal of Building Engineering 70 (2023) 106384.

[36] T. Wang, S. Medepalli, Y. Zheng, W. Zhang, T. Ishida, S. Bishnoi, D. Hou, Z. Shi, Retardation effect of the pozzolanic reaction of low-calcium supplementary cementitious materials on clinker hydration at later age: Effects of pore solution, foreign ions, and pH, Cement and Concrete Research 177 (2024) 107416.

[37] F.P. Glasser, J. Marchand, E. Samson, Durability of concrete - Degradation phenomena involving detrimental chemical reactions, Cement and Concrete Research 38(2) (2008) 226-246.

[38] P.W. Brown, S. Badger, The distributions of bound sulfates and chlorides in concrete subjected to mixed NaCl, MgSO4, Na2SO4 attack, Cement and Concrete Research 30(10) (2000) 1535-1542.

[39] K. De Weerdt, M.B. Haha, G. Le Saout, K.O. Kjellsen, H. Justnes, B. Lothenbach, Hydration mechanisms of ternary Portland cements containing limestone powder and fly ash, Cement and Concrete Research 41(3) (2011) 279-291.

[40] A. Ipavec, T. Vuk, R. Gabrovšek, V. Kaučič, Chloride binding into hydrated blended cements: The influence of limestone and alkalinity, Cement and Concrete Research 48 (2013) 74-85.

[41] Z. Yang, S. Sui, L. Wang, T. Feng, Y. Gao, S. Mu, L. Tang, J. Jiang, Improving the chloride binding capacity of cement paste by adding nano-Al2O3: The cases of blended cement pastes, Construction and Building Materials 232 (2020) 117219.

ISSN: 2414-1895 DOI: 10.6919/ICJE.202604_12(4).0053

[42] M.D.A. Thomas, R.D. Hooton, A. Scott, H. Zibara, The effect of supplementary cementitious materials on chloride binding in hardened cement paste, Cement and Concrete Research 42(1) (2012) 1-7.

[43] M. Balonis, B. Lothenbach, G. Le Saout, F.P. Glasser, Impact of chloride on the mineralogy of hydrated Portland cement systems, Cement and Concrete Research 40(7) (2010) 1009-1022.

[44] J.O. Ukpata, P.A.M. Basheer, L. Black, Slag hydration and chloride binding in slag cements exposed to a combined chloride-sulphate solution, Construction and Building Materials 195 (2019) 238-248.

[45] C. Arya, N.R. Buenfeld, J.B. Newman, Factors influencing chloride-binding in concrete, Cement and Concrete Research 20(2) (1990) 291-300.

[46] Q. Zhu, L. Jiang, Y. Chen, J. Xu, L. Mo, Effect of chloride salt type on chloride binding behavior of concrete, Construction and Building Materials 37 (2012) 512-517.

[47] Z. Yang, J. Jiang, X. Jiang, S. Mu, M. Wu, S. Sui, L. Wang, F. Wang, The influence of sodium sulfate and magnesium sulfate on the stability of bound chlorides in cement paste, Construction and Building Materials 228 (2019) 116775.

[48] R. Jia, Q. Wang, T. Luo, Mechanisms and differences between sodium and magnesium sulfate attacks on alkali-activated phosphorus slag, Construction and Building Materials 403 (2023) 133117.

[49] G. Zhang, M. Li, Z. Zhu, Effect of Aluminium Substitution on Physical Adsorption of Chloride and Sulphate Ions in Cement-Based Materials, Materials (Basel) 16(17) (2023).

[50] Y. Zhao, X. Hu, Q. Yuan, C. Shi, The change of phase assemblage and desorption of bound chloride for seawater cement paste under sulfate attack, Cement and Concrete Composites 139 (2023) 105033.

[51] F. Liu, J. Wang, X. Qian, J. Hollingsworth, Internal curing of high performance concrete using cenospheres, Cement and Concrete Research 95 (2017) 39-46.

[52] L. Huang, P. Yan, Effect of alkali content in cement on its hydration kinetics and mechanical properties, Construction and Building Materials 228 (2019) 116833.

[53] Z. Xu, J. Gao, Y. Zhao, S. Li, Z. Guo, X. Luo, G. Chen, Promoting utilization rate of ground granulated blast furnace slag (GGBS): Incorporation of nanosilica to improve the properties of blended cement containing high volume GGBS, Journal of Cleaner Production 332 (2022) 130096.

[54] J.-f. Wu, F.-y. Qi, J. Zhang, Z.-w. Chen, H.-l. Wang, Q.-f. Liu, Modeling of effect of fly ash amount on microstructure and chloride diffusivity of blended fly ash-cement systems, Construction and Building Materials 443 (2024) 137711.